JOINT EUROPEAN TORUS

JET–P(90)57

M.F.F. Nave, A. Edwards, K. Hirsch, M. Hugon, A. Jacchia,
E. Lazarro, H. Salzmann, P. Smeulders and JET Team

Observation of MHD Structures in JET Temperature Profiles

Observation of MHD Structures in JET Temperature Profiles

M.F.F. Nave[1], A. Edwards, K. Hirsch[2], M. Hugon, A. Jacchia[3], E. Lazarro[3], H. Salzmann, P. Smeulders and JET Team*

JET-Joint Undertaking, Culham Science Centre, OX14 3DB, Abingdon, UK

[1]Laboratorio Nacional de Engenharia e Technologia Industrial, Sacavem, Portugal
[2]Institute F. Plasmaforschung, University Stuttgart, FRG
[3]IFP CNR, Euratom Association, Milan, Italy
[4]IPP, Garching, FRG
** See Appendix 1*

Preprint of Paper to be submitted for publication in
Nuclear Fusion

OBSERVATION OF MHD STRUCTURES IN JET TEMPERATURE PROFILES

M.F.F.Nave[1], A. Edwards, K.Hirsch[2], M.Hugon,
A.Jacchia[3], E.Lazzaro[3], H.Salzmann[4], P.Smeulders

JET Joint Undertaking, Abingdon, Oxon, U.K.

[1]Laboratorio Nacional de Engenharia e Tecnologia Industrial, Sacavem, Portugal
[2]Inst. f. Plasmaforschung,Univ. Stuttgart, F.R.G.
[3]IFP CNR, Euratom Assoc., Milan, Italy
[4]IPP, Garching, F.R.G.

Abstract

Flat regions observed in the profiles of the electron temperature measured by LIDAR Thomson scattering provide some evidence for the existence of helical MHD resistive mode structure in JET discharges. Comparison with profiles of the safety factor q determined from magnetic equilibrium calculations, shows that the most prominent regions are located close to rational values of q. The flat regions are also correlated to perturbations observed with other independent experimental measurements such as soft X-rays, electron cyclotron emission and Mirnov oscillations.

1-Introduction

In a tokamak, the non-linear stage of tearing modes arising from finite resistivity effects are expected to develop magnetic islands at surfaces where the safety factor, q, is rational /1,2/. Theoretical arguments predict that the background axisymmetric profiles of pressure and current could relax locally to a force free configuration with vanishing gradients across the islands /2,3/. The magnetic islands are considered to be responsible for Mirnov oscillations and their unstable evolution is related to disruptions /4/.

Early experimental evidence for flattenings in the temperature profiles was provided by Thomson scattering techniques before disruptions in Pulsator /5/ and in steady state conditions in Wendelstein VII-A /6/. Island structures where further observed in PLT, Wendelstein VII-A and JIPP-TII devices using X-ray tomography /4,7-8/. Perturbations looking like small humps were also observed in the emission profiles of the bremsstrahlung continuum radiation measured in TJ-I /9/.

At JET the development of soft X-ray tomography analysis /10/, electron cyclotron emission (ECE) heterodyne measurements and ECE multichannel spectrometry has provided direct proof of the flattening of X-ray emission and temperature profiles in events associated with disruptions and with partial sawteeth. Island structures and flattening of the profiles were seen located at q=1 associated with partial sawteeth /11/, and located at q=2 associated with events preceding a disruption /10,12-14/.

More recently, the electron temperature and pressure profiles measured in JET with the new LIDAR-Thomson scattering system /15,16/ showed that regions of reduced slope occur very often and can be associated with a variety of mhd activity in non-disruptive conditions /17/. Comparison with the safety factor profiles obtained from the solution of the magnetic equilibrium problem from measured magnetic signals /18,19/, has shown a correlation between the location of low order rational q values and localized flat regions of the electron temperature /17/. Perturbations at the same radial positions are also seen by soft X-rays and ECE diagnostics for the data analysed and are at the same time visible on external magnetic probes. At JET magnetic oscillations are observed with frequencies ranging from zero (locked modes) to around 10kHz. From the analysis of the magnetic data the poloidal and toroidal mode numbers can be determined as well as the location of the 'O' and 'X' points /13/.

Unlike methods of mode analysis requiring line inversion techniques the LIDAR and ECE diagnostics provide a direct local measurement of the profile structure of JET discharges. Here we discuss results obtained with the LIDAR system. The LIDAR system has some advantages over conventional Thomson scattering systems in the detection of flat regions since it uses the same set of detectors and thus the same set of calibration constants for measurements

at different radii. This eliminates spurious flat regions caused by interspatial channel calibration errors. With the LIDAR system one effectively takes a snapshot of the temperature profile, with an exposure time of ~7nsec. As several flat regions (each one associated with a different value of q rational) can be observed simultaneously, the LIDAR profiles may provide an immediate insight into the magnetic topology of the JET plasma. However, since at present the LIDAR profiles have a spatial resolution of 9cm, we will restrict our analysis to large perturbations that are outside the error bars caused by photon statistics.

In what follows, data analysis showing the correlation between the LIDAR measurements and the data obtained from several other diagnostics is presented. In section 2, we discuss examples of individual discharges with T_e profiles which clearly exhibit flat regions associated with a range of mhd activity with low order poloidal and toroidal mode numbers (m,n). In general, several flat regions are observed simultaneously, however, for the sake of clarity, perturbations related to different mode numbers are discussed separately. In section 3, we discuss the conditions where smoother LIDAR profiles have been observed. Finally, in section 4, we show the results of a statistical analysis involving 1988 JET discharges, which shows the correlation of the temperature profile perturbations with rational q values. Details of the LIDAR system and a series of measurements carried out to check for possible spurious profile effects are given in the appendix.

2 - Analysis of individual discharges exhibiting large flat regions in the temperature profiles

2a - A general view

LIDAR T_e profiles, measured in the equatorial plane of JET, are in general non-smooth, showing changes of inflection, flat regions and in some cases humps, at several radial positions. Examples already published by Bickerton et al. /20/ show that non-smooth temperature profiles are observed under a variety of operational conditions, occurring both with ohmic and auxiliary heating. The shape of a perturbation is quite often within the experimental error, therefore in this paper we will always refer to a perturbation as a

'flat region'. For most of the large flat regions, i.e. outside the experimental error, a correlation with MHD activity is found, as will be shown in the examples below.

The actual nature of the mhd activity associated with the flat regions may change, however, as the discharge evolves in time. Magnetic measurements show that with ohmic heating the current rise is characterized by two phases /21/. Early in the discharge, usually within the first seconds, the magnetic signals show distinct peaks in time closely related to rational values of the edge safety factor, with modes that have a $m=q_a.n$ with n=1 or n=2 symmetry. In this phase, the plasma profiles (e.g. current density, q profiles and electron temperature) are either hollow or flat and the mhd activity observed is thought to be caused by double-tearing or edge kink modes. Later on, as current penetration occurs, and the profiles become peaked, a less clear MHD spectrum is observed, sometimes showing peaks no longer correlated to integral values of q_a. The discharge is then in a regime where tearing modes may be unstable /21/. As the current penetration continues, q_o decreases to a value around or below unity, coinciding with the appearance of sawtooth activity. A typical JET discharge is then in the current flat top phase and from then on, the characteristics of the mhd activity observed depends on the operation conditions, e.g. on details of the auxiliary heating used, whether pellets are injected, etc.. However, independent of the conditions, for the remainder of the discharge the most important modes observed are those with low mode numbers: (1,1), (2,1) and (3,2).

A LIDAR T_e profile which clearly exhibits large perturbations, which can not be explained by experimental uncertainties, is shown in fig.1. The error bars indicate one standard deviation and are due to the photo electron statistics of the raw LIDAR signals. This profile was taken during ICRH heating, 130ms after a sawtooth crash, when the center of the plasma has already been reheated. Also shown in the figure are the positions of rational values of q. (The q profiles at the time of the LIDAR measurements are obtained by the calculation of the magnetic equilibrium which best fits the experimental magnetic signals). The figure indicates a possible correlation between the positions of rational values of q and the positions of the observed flat regions. This correlation is subject to an error in the calculated q profile varying between ±15% in the center and 0% at the edge leading to a variation

in the q=1 radius of ±10cm. This is combined with an uncertainty of 3cm on the LIDAR profile absolute position, and a spatial resolution of 9cm due to the response time of the detection system and the laser pulse length. Nevertheless, the statistical analysis discussed later confirms the above correlation. ECE data also show the existence of a large flat region around the sawtooth inversion radius, coinciding in position with the central flat region seen in the LIDAR profile, while the magnetic pick-up coils indicate the presence of rotating n=1 and n=2 modes.

The LIDAR profiles are currently available only at intervals greater than 1 second and therefore it is not possible to study in detail the evolution in time of the size of the T_e plateaus, except in the special cases of locked modes which can last upto several seconds.

Figure 2 shows the T_e and q profiles obtained at two different times and operational regimes for the same discharge. Information about the discharge and the magnetic perturbation measurements are shown in Figure 3. One profile in figure 2 with the higher central q value has been taken at the beginning of the current flat top during the OH phase. The other profile has been measured during the additionally heated phase in the discharge. One can see a modest expansion of the q=2 surface by 10cm on the high field side from 2.4 to 2.3 m between those times, which also ocurs for the flat region in the LIDAR profile close to this surface.

Figure 3 shows that the T_e profile at t=4s was taken before the appearance of sawteeth in the ohmic regime. The T_e profile at t=10s, was measured at the beginning of a 'monster sawtooth', i.e. a sawtooth free period followed by a large sawtooth collapse/22/, which started when combined NBI and ICRH heating was applied. In this particular case, the amplitude of the n=1 activity is 5-10 times larger than is normally observed during a 'monster sawtooth'. (Sawtooth free periods will be discussed further in section 3). Analysis of the magnetic pick-up coils data shows the presence of two n=1 modes, one with the frequency of the plasma central rotation (a broad spectrum does not allow for an unambiguous identification of the poloidal number), and an edge mode with a lower frequency identified as an m=4. The ECE data, just before the sawtooth free period, show a sawtooth inversion radial position of 3.45m, in agreement with the q=1 position and the location of the central perturbation

observed in the T_e profile.

An indication of the type of modes observed may be obtained by plotting the trajectory in time of the discharge in the (q_o,q_a) plane /21/. Figure 4 shows such a trajectory for the current rise and flat top phases for the discharge presented in the figures 2 and 3. Also indicated are the simplified boundaries of various MHD instability regions calculated using a cylindrical model in circular geometry /23/. It should be noted that the profiles shown in figure 2 are associated with a section of the trajectory in the (q_o,q_a) plane lying entirely in the so-called tearing-mode region and therefore the presence of magnetic island may be expected. If tearing modes are excited, flat regions in T_e may become visible, provided the positions of the islands have the correct orientation with respect to the line of observation.

In the previous examples, the central flattenings associated with the m=1, n=1 modes are seen on both sides of the profiles. It is not always possible to distinguish between the effects of an island or a partial sawtooth crash leaving behind a symmetric ring of flat temperatures /11/. However, often only one central m=1 structure is observed, which changes sides as the mode rotates, as will be shown below.

These examples also show that the perturbations are wider on the inside of the profiles, i.e. on the high field side. This is generally observed and is consistent with predictions of tearing mode theory in toroidal geometry /24,25/. Numerical simulations with the FAR code show that for the m=2, n=1 mode, a factor of 2 could be expected between the inside and the outside island widths /25/. This, the spatial resolution of the LIDAR system and the orientation of the islands with respect to the measurement may explain why in some profiles (as the profile at t=10s in fig.2) the perturbations are hardly visible on the low field side and why there is a lack of symmetry for the flat regions around q=2. Statistical analysis, discussed later, actually shows that in most cases the m=2 perturbations are observed simultaneously on both sides of the profile.

Due to the fact that the magnetic lines are packed close together on the outside, because of the Shafranov shift, and due to the finite spatial resolution of the measurement, an apparent overlap may occur between two

adjacent rational surfaces. This can put the region of reduced slope, spatially as well as in absolute temperature, in between the rational surfaces. In addition, the errors in the positions of the temperature profiles and the positions of rational q, can cause an apparent lack of isothermality between flat regions with the same mode numbers observed on the inside and the outside. However, plots of T_e versus q, obtained by interpolating q at the same radial positions as the T_e profile, show that isothermality is verified within 10%.

The following examples of rotating and quasi-stationary modes will illustrate further the correlation between the T_e LIDAR profiles and data from other diagnostics.

2b - Observation of m=1, n=1 modes

At JET SXR and ECE have shown the presence of m=1, n=1 islands under various conditions, often coupled to either rotating or locked modes with m≥2, visible on the magnetic signals. They are observed following partial sawtooth collapses, and in several cases seem to decay into an annular region /11/. Sometimes in auxiliary heated discharges, m=1, n=1 structures with the frequency of rotation of the central plasma are observed throughout the sawtooth cycle, although apparently not being involved in the sawtooth collapse /23,26/. They have also been linked with fishbone activity /27/.

The flattenings of the LIDAR temperature profiles around q=1, observed in those cases, are likely to be associated with a helical m=1, n=1 mode. In the particular case of the partial sawtooth, some flat regions observed in the LIDAR profiles (and also with SXR and ECE data) correspond to an annular region. The MHD activity responsible for this annular region has decayed away several milliseconds before the temperature profile has been measured.

In addition, depressions of the temperature located at the sawtooth inversion radius are seen after multiple pellet injection and are associated with 'snakes' /28/. The snake is a local density perturbation, normally located at the q=1 surface, although it has also been found in JET at the q=1.5 surface /29/ and in the WVII-A machine at the q=2 surface /30/. This indicates that when the 'snake' is present, the plasma is in a different helical equilibrium

from that normally found in JET plasmas.

An example of a central flattening observed after a sawtooth collapse was shown in figure 1. We will now discuss the example of a rotating m=1,n=1 mode apparently not associated to the sawteeth crashes. The case of a quasi-stationary m=1 mode coupled to an m=2 will be discussed in the next section.

In this example, a radio-frequency heated discharge (I_P=3MA, B_ϕ=3.4T, P_{RF}=7MW) shows oscillations, interpreted as continuous fishbone activity /27/, with a nearly constant amplitude and frequency of 0.5 kHz both in soft X-rays (in figure 5a) and ECE signals. These oscillations, are observed prior to the sawteeth collapses, however their constant amplitude indicates that the sawtooth collapse is independent of them. (The mhd activity observed in this discharge is described in more detail elsewhere /27/.)

Figure 5b shows the T_e and q profiles obtained. The large flat region close to the q=1 surface indicates the presence of an m=1 perturbation. From SXR measurements the toroidal mode number has been seen to be n=1. Phase reversals of the SXR signals indicate an m=1 mode in the center, with an m=2 and probably m=3 at the outside, at the positions of rational q seen in fig.5b. The reconstruction of the soft X-ray midplane emission profile shows an m=1 flattening coinciding with that of fig.5b, while the soft x-ray tomography of the central plasma zone, in fig.5c, shows an m=1 island related to the q=1 surface. The mapping of the ECE signals for a full oscillation period on the poloidal plane, in figure 5d, also shows an m=1 perturbation at the position of q=1. (The different phases of the m=1 perturbation shown in the figures, can be accounted for when we consider the mode rotation and the toroidal locations of the different diagnostics.)

2c - Observation of m=2, n=1 modes

Large amplitude rotating or locked modes, usually with mode numbers (2,1) or (3,2), are observed under many operating conditions and may persist for many seconds. In particular, locked or quasi-stationary (slowly rotating) modes can appear early in the current rise, or after perturbations such as pellet injection or a large sawtooth collapse occurring after a period of sawtooth

suppression /31/. Locked (2,1) modes are also the main precursor for disruptions /14/.

We discuss a quasi-stationary mode which appeared after a 'monster sawtooth' crash (I_P=2MA, B_ϕ=2.1T, P_{RF}=4MW). The signals from magnetic pick-up coils, in figure 6a, show a slow oscillation of 4.25Hz with a saturated amplitude. Magnetic data analysis indicated a dominant m=2,n=1 structure /32/. The same frequency was also measured with the different channels of ECE and SXR diagnostics suggesting a toroidal coupling /32/ between external and central modes.

The T_e and q profiles obtained at two different times are shown in figure 6b. As in the previous examples, an obvious flat region is seen in the T_e profiles close to the q=1 and the sawtooth inversion radii. Another large flat region is seen close to q=2 on the inside of the profile taken at t=12s. On the earlier profile, at t=10s, the flatter structures close to q=2 have widths inside the experimental error, however, their position, symmetry and temperature value when compared to the t=12s profile, indicate that they may be caused by an m=2, n=1 mode.

The magnetic signals show that between the two T_e profiles there is an 180° phase difference. The magnetic analysis provides the toroidal location where the 'O' points of the n=1 rotating islands are in the mid-plane, on the low-field side. Thus, the poloidal location at the toroidal location (ϕ=0°), where the instantaneous LIDAR measurements are made, can be obtained from the magnetic signals under the assumption of mode coupling of all n=1 modes /33/. If we assume that the m=2, n=1 mode is coupled to a central m=1, n=1 mode, we find that the m=1 perturbations on the two T_e profiles shown, are in fact observed at the positions expected on opposite sides of the profiles /32/.

Soft X-ray tomography confirms the existence of islands of low poloidal m numbers, m=1 and m=2, located at the identified rational q surfaces. Some activity is also seen around the q=1.5 surface and is likely to be an m=3, n=2 mode. Figure 6c shows the reconstructed emission profiles around q=2 It illustrates what is usually observed in the temperature profiles, that the radial extent of the perturbation is greater on the inner side. Due to this inside/outside asymmetry the perturbation may be only clearly visible on the

inside. It can explain why the m=2 mode is sometimes asymmetric on the LIDAR profiles. The figure also shows the rotation effect on the observed width which is a maximum when the 'O' point of the island is in full view.

The maximum width of the perturbation, observed on the inner side of the SXR emission profiles, is ~20cm. The inner side of the LIDAR profile at t=12s shows a flattening around q=2 with a width of 10-15cm. The difference between the widths observed can be explained by a phase difference, since the LIDAR and SXR measurements are taken at different octants. Comparable widths are also estimated from the magnetic signals and from tearing mode calculations. From the amplitude of the m=2, n=1 oscillation measured in the magnetic signals, and assuming that the radial perturbed field varies with radius as $(r)^{m+1}$, one can estimate an island width of ~20cm at the position where q=2. From a numerical simulation of the tearing mode problem in the cylindrical approximation /23/, where we used the experimental current density profile at t=12s, we calculated that the m=2, n=1 mode would saturate with an island width of ~17cm.

2d - Observation of m=3, n=2 modes

Modes with toroidal number n=2 are also seen in many operating conditions, often already during the current rise phase. Enhanced n=2 activity is measured at particular conditions, such after pellet injection /34,35/ and after a 'monster sawtooth' collapse /22/. In some high-β discharges the β collapse is associated to n=2 and n=3 activity /36/.

The correlation between T_e perturbations at q=1.5 and the observation of m=3, n=2 modes with other diagnostics is particularly clear in discharges with pellet injection. Examples have already been presented in the JET literature, so we will refer here to a pulse analyzed in reference /35/. It showed that pellet injection during the current rise of limiter discharges, is followed by a sharp increase in the n=2 mhd activity. Soft X-ray analysis indicated a poloidal mode number of m=3, while the emission profiles showed a flattened region around the q=1.5 surface. Flatter regions at the same position were seen in the LIDAR temperature and pressure profiles.

It should be noticed that in the data examined to date, the m=3, n=2 modes appear to affect the T_e profile to a similar extent as the m=2, n=1 mode. The cylindrical approximation, however, predicts widths one order of magnitude smaller. Toroidal effects /37/ may have to be invoked in order to explain the m=3, n=2 island widths suggested by the temperature profile observations.

3 - Smoother temperature profiles

Smoother LIDAR T_e profiles are measured in some conditions where a reduction of MHD activity is observed. Most noticeable are the smooth central regions after pellet injection and the smooth outer regions after an L to H transition. A lack of large profile structures has also been observed during periods of sawtooth stabilization. Part of this effect is certainly also due to a better photon statistic due to the higher electron density in pellet fueled and H-mode discharges. However error bars are taken into account in our analysis.

(i) discharges with pellet fueling

Pellet injection in the current rise phase of limiter discharges, has the effect of keeping q_o above unity and consequently delaying the appearance of sawtooth activity /35/. After the pellet injection, the T_e profiles show smooth central regions, in agreement with the absence of m=1,n=1 modes.

(ii) discharges with H-mode

Smooth LIDAR T_e profiles are observed during the H-phase /38/ of some JET discharges where the L to H transition is followed by a decrease of MHD activity. In those cases the T_e profiles still show central perturbations around q=1 as one would expect, since usually sawtooth activity is not suppressed, but are very smooth on the outer regions indicating a reduction of internal modes with m>1.

To illustrate this, figures 7a-b show an ELM dominated H-mode, where the n=1 activity measured with the magnetic pick-up coils is decreased by a factor of 10. The LIDAR T_e profiles show smooth outer regions. (In this particular

example the T_e profiles where available soon after sawtooth crashes and therefore are flat in the central region.)

However, not all H-modes are accompanied by a decrease in mhd activity. Clear counter examples are H-regimes occurring for values of the toroidal β parameter close to the Troyon limit, which show large amplitude n=1, such as fishbones and sometimes enhanced n=2 and n=3 activity /36/. As in the examples in the previous section, the T_e profiles show large structures that can be correlated to perturbations observed in SXR and ECE signals.

(iii) Discharges with 'monster sawtooth'

Sawtooth stabilization with $q_o<1$ is obtained in JET, with high power additional heating, for periods lasting up to 5s. The level of coherent MHD modes is low as reported in reference 22 and is in the order of $\delta B/B \leq 10^{-4}$.

As a general trend, the LIDAR temperature profiles obtained during the temperature saturation phase of sawtooth free periods do not show large perturbations, but exceptions do occur as is the case for the early phase of the 'monster sawtooth' shown in figure 2. Some exceptions may also be explained by the presence of fishbones, which have been observed occasionally during 'monster sawteeth' /27/.

4 - Statistical comparison with results of equilibrium analysis

In order to investigate the correlation between the q profiles and the perturbations in the T_e profiles, a numerical method was used to analyze statistically the complete set of 1988 LIDAR data. A movable grid was used to sample the local slope of the temperature profile. A selection criterion has been used which records an observation when the change in gradient is outside the temperature profile error bars. The R coordinates of the points of minimum slope thus obtained are recorded. These observations were subsequently compared with the position of the rational q surfaces. This comparison is shown in contour plots in the (q, R) plane. A grid cell corresponding to intervals $\Delta q=0.1$ and $\Delta R=0.05$m is used to plot the frequency of observations.

Figure 8 shows the contour plots for the lower field side, obtained for the

most reliable data (in LIDAR profiles characterized by the error $\delta T_e/T_e<0.2$ everywhere and q profiles characterized by the systematic consistency checks on the magnetic data being satisfied /19/.). Note the correlation of the observations with discrete values of q, around q=1, q=3/2 and q=2. A similar result is obtained for the high field side. Most of the profiles in the database were measured during the plasma current flat top phase when the q profiles of JET discharges are very similar and very steep in the low field side due to the aspect ratio. This explain the small spread in radius observed in figure 10. (Electronic tests designed to check whether the bunching of the data in R could be an artifact of the LIDAR system, are described in the appendix.)

The statistical analysis confirms that the presence of flat T_e regions at rational values of q on both the inside and outside of the profile is not a random event. The correlation between the occurrence of flat regions near to q=1 and q=2, on the inside and outside of T_e profiles was studied. As expected from the symmetry of MHD perturbations, the observation of q=1 plateaus on the inside and the outside is not correlated, while the observation of q=2 plateaus appearing simultaneously on both sides is correlated. A further result was that q=1/ q=2 flattenings on the inside/ outside are anti-correlated with the observation of q=2/ q=1 flattenings on the outside/ inside. This can be explained by the well-known phase-coupling of the (1,1) and (2,1) modes in tokamaks /33/.

5- Summary

Comparison between typical LIDAR T_e profiles in the equatorial plane of JET and the q profiles determined from magnetic equilibrium calculations shows that the location of flatter regions of T_e are correlated with rational values of q. The existence of perturbations located at the q rational surfaces is further confirmed by soft X-rays, ECE and magnetic data analysis.

The flat regions are seen on most modes of JET operation and can be associated with many types of MHD events seen in the signals of other diagnostics. In most cases studied, the flattenings in T_e can be associated to the observation of magnetic islands. In JET, large magnetic islands can be very long-lived and

are observed under many operating conditions. The most important ones have low mode numbers (1,1), (2,1) and (3,2).

Locked and quasi-stationary modes, in particular, may appear early in the current rise and remain present for most of the remaining of the discharge. In those cases, the flat regions observed in the temperature profiles have a behaviour consistent with that of magnetic islands caused by nearly saturated resistive modes. In the special case of m=1, not all flattenings observed in T_e around q=1 are associated with islands but also with annular regions.

In particular situations, when certain types of MHD activity are known to be reduced, the LIDAR T_e profiles are observed to be smoother. Examples are the profiles measured after pellet injection, during 'monster sawteeth' and after a transition into an H-mode. The pellet injection has the effect of suppressing sawtooth activity and consistently the temperature profiles are very smooth in the central region. During some H-modes, the external region of the profiles become smooth, in agreement with a reduction of MHD activity with m>1.

Although at present, the time evolution of the T_e profiles cannot be monitored by LIDAR in a short time scale, the observation of flattenings at several different times during the same discharge shows that flat structures are present during much of the discharge. In most cases data analysis from other diagnostics shows the presence of MHD modes at the time of the temperature measurements. However, sometimes the flat regions in the temperature profiles are seen as result of MHD activity which may already have decayed away, as in the case of the annular regions observed after a partial sawtooth collapse. (An upgrade of the LIDAR system will increase the time resolution of future measurements).

The statistical analysis shows that the simultaneous appearance of flat regions at q=2 on the inside and the outside of a T_e profile is not a random event. However, consistent with the fact that in toroidal geometry with large Shafranov shift the 'X' and 'O' points of an island are not poloidally equidistant /24/, the flattening of modes with even parity is sometimes seen on one side only of the T_e profile in the equatorial plane. Naturally this also occurs for odd parity, and it was confirmed to be the case for most

perturbations around q=1.

A further result from the statistical analysis presented was that the observation of a q=1 plateau on the inside of the temperature profile is anti-correlated to the observation of a q=2 plateau on the outside. This implies a phase relation between the modes which may be explained by mode coupling.

It is generally observed that the LIDAR T_e plateaus are wider on the high field side. This is consistent with what is observed in the soft X-rays emission data and magnetic analysis with the FAR code /25/ for a toroidal JET plasma

The width of the flattenings observed in the temperature profiles is consistent with the size of perturbations measured with other diagnostics. It should be noticed that in the data examined to date, the m=3, n=2 mode appears to affect the T_e profile to a similar extent as the m=2, n=1 mode.

To conclude, we have presented a significant correlation between perturbations in the temperature profile data and the mode analysis from independent experimental measurements. These temperature profile perturbations occur in most discharges, in all kinds of plasma conditions.

Acknowledgements

The authors wish to thank Dr. R.Galvao for useful comments, Dr.D.Campbell and the ECE group for assistance with ECE data, Mr. C.Gowers for the many discussions and help with the LIDAR data and Dr D.Ward for help with the analysis of magnetic data.

Appendix

The LIDAR diagnostic uses a time-of-flight technique to infer spatial profiles from time varying signals. Thus electronic ringing in the detector signals for the different spatial channels, could lead to deviations from a smooth profile and if present, this would occur more frequently at certain radii than at others. Since the majority of JET discharges show spatial q profiles located

inside a certain band, the bunching of observations in the major radius, R, domain would also lead to bunching in the q domain. To investigate this problem a test experiment was carried out to illuminate the photodetectors with an optical square pulse. The 350ps duration ruby laser pulse, normally used for Thomson scattering, was passed through open air over a distance of 2.5m about 6m away from the detector. Mie scattering from dust particles and Rayleigh scattering from air both contribute to the observed scattering signal. No ringing with the characteristic frequency close to that corresponding to the observed spatial bunching at 3.8,3.4,2.8 and 2.4m was found on the fast rise signal.

The spatial resolution of the diagnostic, determined by the combination of the laser pulse duration and the response time of the detection system was improved to about 9 cm by using a signal deconvolution technique. A confidence check on this fast converging numerical procedure was carried out by comparing its results with those from a commercially available (but slow) maximum entropy deconvolution software package. The results were in complete agreement.

References

/1/ White, R., Monticello, D. A., Rosenbluth, M., and Waddell, B. V., Phys. Fluids **20**, (1978) 800

/2/ Bateman, G. and Morris, R. N., Phys. Fluids **29**, (1986) 753

/3/ Battacharjee, A., Glasser, A. H., Avinash, Sedlak, J. E., Phys.Fluids **29**, (1986) 1

/4/ Sauthoff, N. R., Von Goeler, S. and Stodiek, W., Nucl. Fusion **18**, (1978) 1445

/5/ Bartlett, D., Cannici, G., Cattanei, G. et al., in Plasma Physics and Controlled Nuclear Fusion Research 1980 (Proc. 8th Int. Conf., Brussels, 1980) vol.1, IAEA, Vienna (1981) 173

/6/ Jaenicke, R.and W VII-A Team, Nucl. Fusion **28** (1988) 1737

/7/ Tsuji, S., Nagayama, Y., Kawahata, K., Noda, N. and Takahashi, S., Nucl. Fusion **22**, (1982) 1082

/8/ Smeulders, P., Report IPP-2/252 (1983)

/9/ Pardo, C., Zurro, B., and the TJ-I team, in Controlled Fusion and Plasma Heating (Proc. 13th Eur. Conf. Schliersee, 1986), vol. 10C, part I, European Physical Society (1986) 117

/10/ Granetz, P. and Smeulders, P. Nucl. Fusion **28**, (1988) 475

/11/ Westerhof, E. and Smeulders, P., Nucl. Fusion **29** (1989) 1056

/12/ Salmon, N. A., Bartlett, D. V., Costley, A. E. and Hugon, M., in Controlled Fusion and Plasma Physics (Proc. 14th Eur. Conf. Madrid, 1987), vol. 11D, part III, European Physical Society (1987) 1248

/13/ Snipes, J. A., Campbell, D. J., Haynes, P. S. et al., Nucl. Fusion **28**, (1988) 1085

/14/ Wesson, J. A., Gill, R. D., Hugon, M. et al., Nucl. Fusion **29**, (1989) 641

/15/ Salzmann, H., Hirsch, K., Nielsen et al., Nucl. Fusion **27**, (1987) 1925

/16/ Salzmann, H., Bundgaard, J., Gadd, A. et al., Rev. Scientific Instruments **59**, (1988) 1451

/17/ Nave, M. F. F., Lazzaro, E., Gowers,C. et al., in Controlled Fusion and Plasma Heating (Proc. 15th Eur. Conf. Dubrovnik, 1988), vol. 12B, part I, European Physical Society (1989) 441

/18/ Blum, J., Gilbert, J. C., Le Foll, J. L.,and Thooris, B., Proc. 8th Europhys. Conf. on Comput. Phys. Eibsee 1986, vol.10D, (1986) 49

/19/ Lazzaro, E. and Mantica, P., Plasma Phys. Contr. Fusion **30**, (1988) 1735

/20/ The JET team, in Plasma Physics and Controlled Nuclear Fusion Research1988 (Proc. 12th Int. Conf., Nice, 1988) vol.1, IAEA, Vienna (1989) 41

/21/ Campbell, D. J., Lazzaro, E., Nave, M. F. et al., Nucl. Fusion **28**, (1988) 981

/22/ Campbell, D. J., Start, D. F. H., Wesson, J. A., et al., Phys. Rev. Lett. **60**, (1988) 2148

/23/ Wesson, J. A., Nucl. Fus. **18**, (1978) 87

/24/ Fussmann, G., Green, B. J. and Zehrfeld, H. P., in Plasma Physics and Controlled Nuclear Fusion Research 1980 (Proc. 8th Int. Conf., Brussels, 1980) vol.1, IAEA, Vienna (1981) 353

/25/Hender. T. C., Robinson, D.C. and Snipes, J. A., in Plasma Physics and Controlled Nuclear Fusion Research 1986 (Proc. 11th Int. Conf. Kyoto 1986), vol.1, IAEA Vienna (1987) 291

/26/ Campbell, D. J., Edwards, A. W. and Pearson, D., in Controlled Fusion and Plasma Physics (Proc. 16th Eur. Conf. Venice, 1989), vol.13B, part II, European Physical Society (1989) 509

/27/ Nave, M. F. F. et al, Fishbone activity in JET, submitted to Nucl. Fusion (1990)

/28/ Edwards, A. W., Campbell, D., Cheetham, A. et al., in Controlled Fusion and Plasma Heating (Proc. 15th Eur. Conf. Dubrovnik, 1988), vol. 12B, part I, European Physical Society (1988) 342

/29/ Weller, A.,Cheetham, A. D., Edwards, A. et al., Phys. Rev. Lett. **59**, (1987) 2303

/30/ Weller, A., Brakel, R., Bushenn, R., et al., in Controlled Fusion and Plasma Physics (Proc. 16th Eur. Conf. Amsterdam, 1990), vol. 14B, part II, European Physical Society (1990) 479

/31/ Snipes, J. A., Campbell, D. J., Hender, T. C., Von Hellermann, M., and Weisen, H., Nucl. Fusion **30**, (1990) 205

/32/ Snipes, J. A., Campbell, D. J., Hugon, M. et al., in Controlled Fusion and Plasma Heating (Proc. 15th Eur. Conf. Dubrovnik, 1988), vol. 12B, part I, European Physical Society (1988) 346

/33/ Karger, F., Lackner, K., Fussmann, G. et al., in Plasma Physics and Controlled Nuclear Fusion Research 1976 (Proc. 6th Int. Conf., Berchtesgaden, 1976) vol.1, IAEA, Vienna (1977) 267

/34/ The JET team, in Plasma Physics and Controlled Nuclear Fusion Research 1988 (Proc. 12th Int. Conf., Nice, 1988) vol.1, IAEA, Vienna (1989) 215

/35/ Huysmans, G. T., Galvao, R. M. O., Goedbloed, J. P., Lazzaro, E. and Smeulders, P., Plasma Phys. and Contr. Fusion **31**, (1989) 2101

/36/ Smeulders, P., Adams, J. M., Balet, B. et al, in Controlled Fusion and Plasma Physics (Proc. 17th Eur. Conf. Amsterdam, 1990), vol. 14B, part I, European Physical Society (1990) 323

/37/ Edery, D. et al., EUR-CEA-FC-1109 (1981)

/38/ Balet, B., Boyd, D., Campbell, D. J. et al. , High temperature L and H mode confinement in JET, JET-P(89)81 (1989)

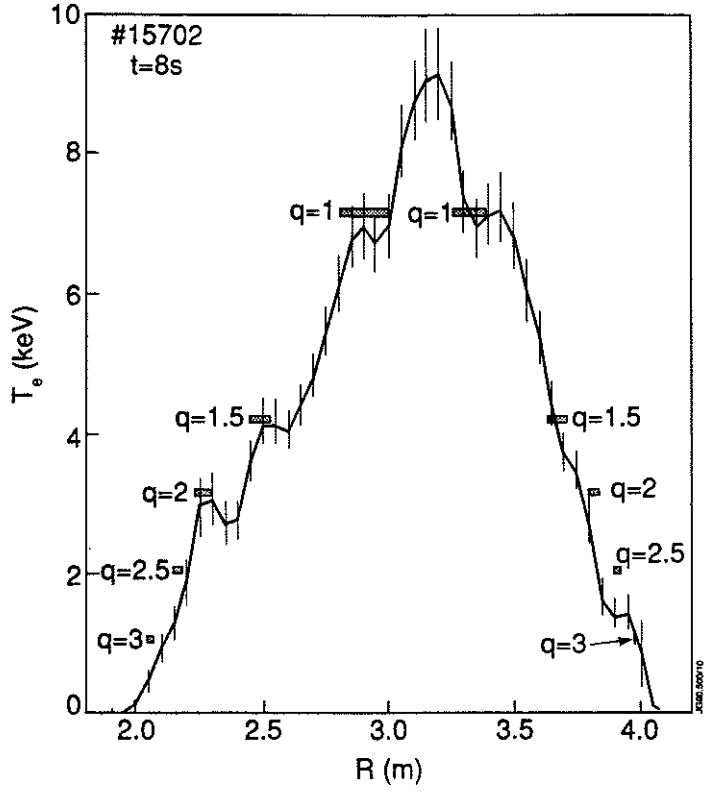

Figure 1 - A LIDAR T_e profile showing large perturbations. The boxes indicate the positions of rational q surfaces and their spatial uncertainty.

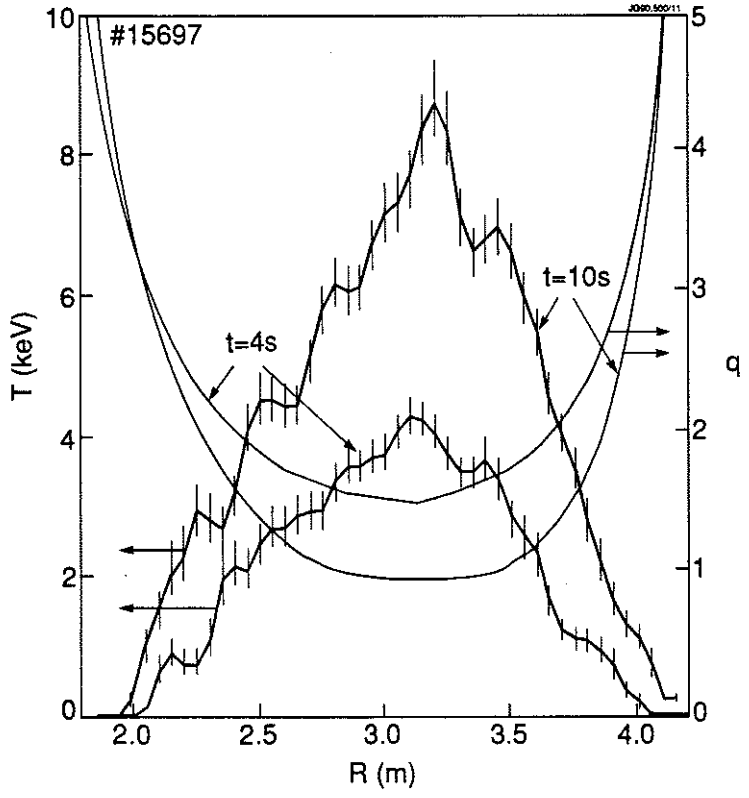

Figure 2 - T_e and magnetically identified q profiles at different times as a discharge evolves through the current flat top.

a) t= 4 sec,

b) t=10 sec.

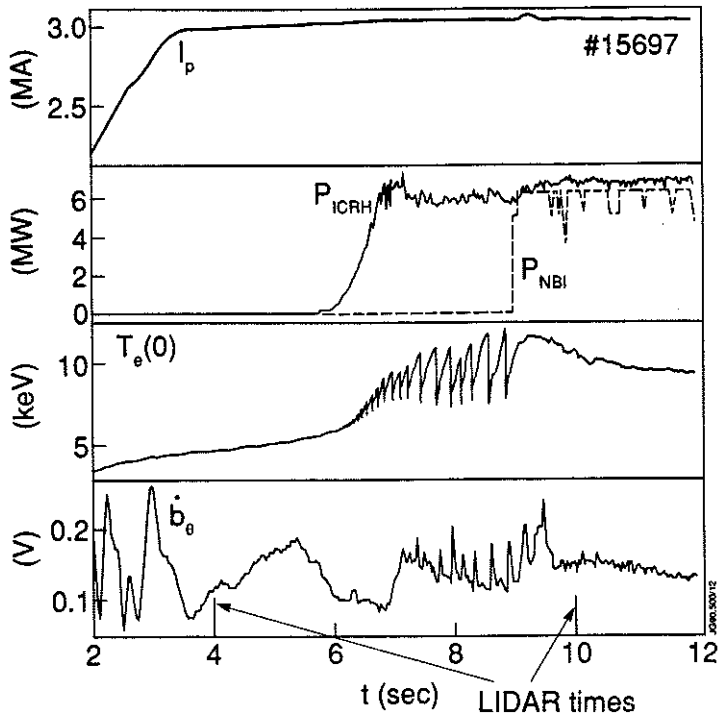

Figure 3 - Time behavior of plasma parameters for the discharge shown in figure 2. (i) total plasma current,

(ii) auxiliary heating power,

(iii) central temperature,

(iv) time derivative of the perturbed poloidal magnetic field (from a n=1 combination of pick-up coil signals measured at 45° above the mid-plane on the lower field side).

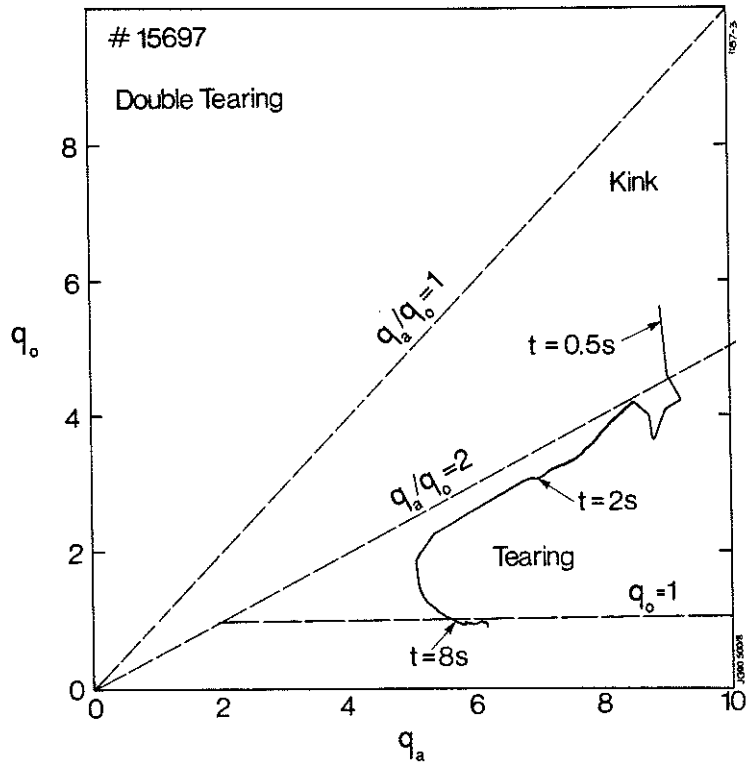

Figure 4 - Trajectory in the (q_0, q_a) plane for pulse 15697.

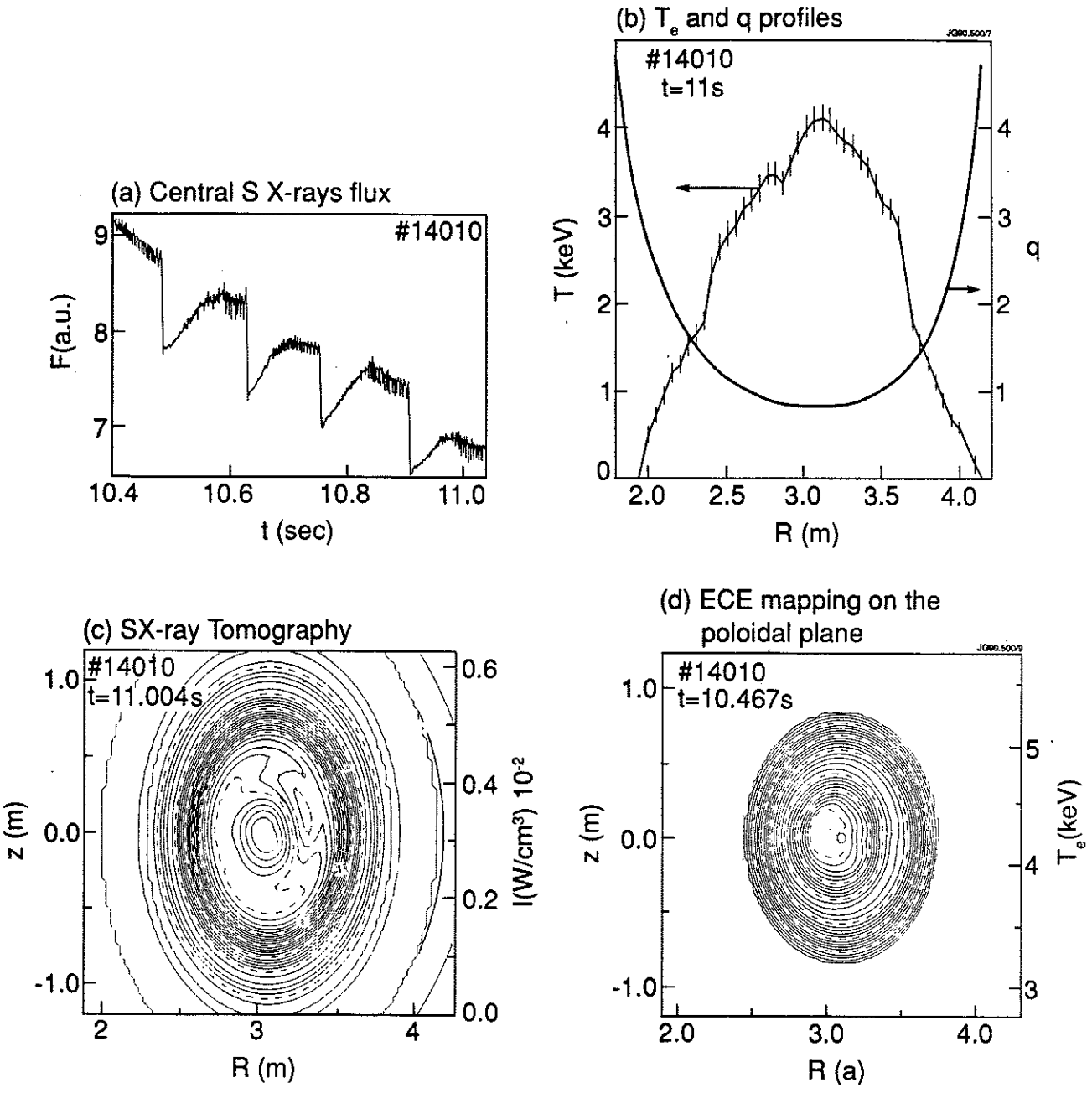

Figure 5 - Observations of a rotating m=1,n=1 mode.

a) - Central soft X-ray flux amplitude vs time showing the evolution of a perturbation rotating at 400Hz.

b) - T_e and q profiles.

c) - Soft X-ray tomography of the central plasma zone.

d) - Mapping of ECE measurements on a poloidal cross-section. (N.B. SXR and ECE measurements with the required time resolution were not available for the same time. However, one can see from a) that the central perturbations obtained in c) and d) can be associated to the same type of oscillation.)

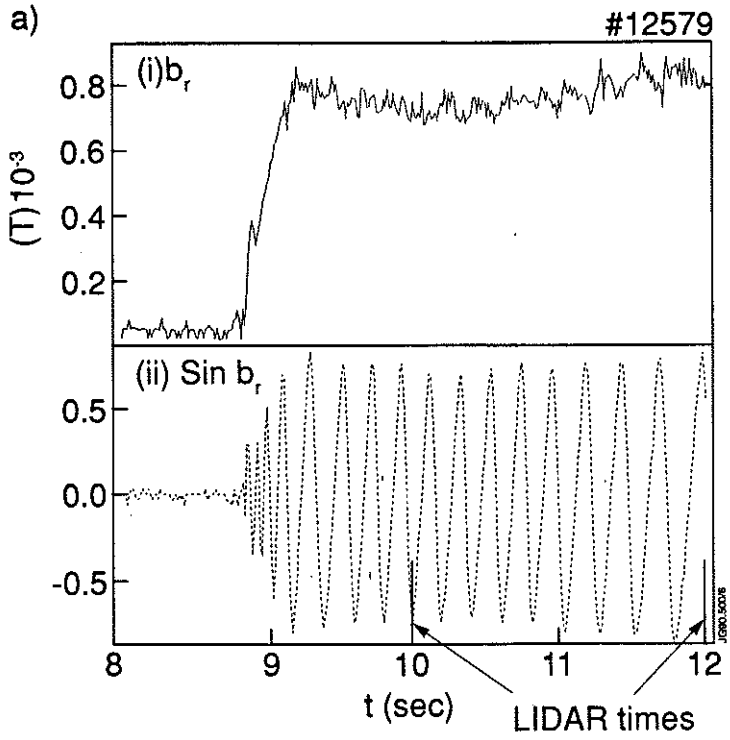
a)
#12579
(i)b$_r$
0.8
0.6
0.4
0.2
(T)10^{-3}
(ii) Sin b$_r$
0.5
0.0
-0.5
8
9
10
11
12
t (sec)
LIDAR times

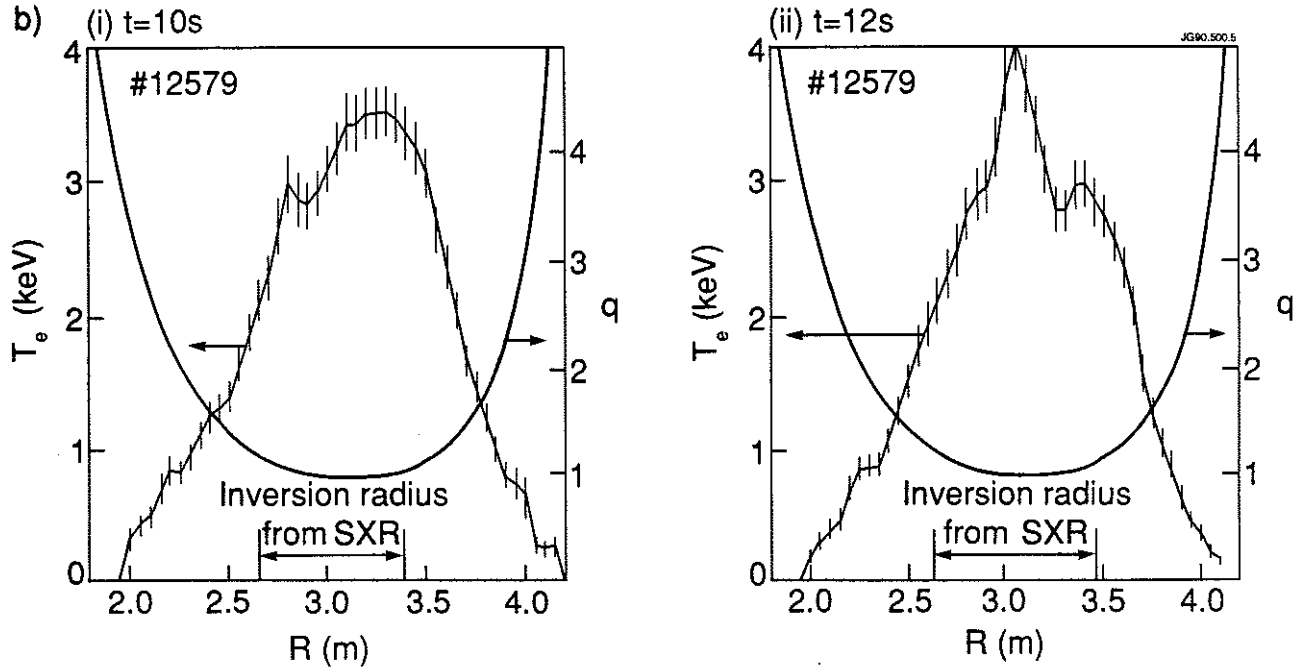
b)
(i) t=10s
#12579
T$_e$ (keV)
q
Inversion radius
from SXR
R (m)
(ii) t=12s
#12579
T$_e$ (keV)
q
Inversion radius
from SXR
R (m)

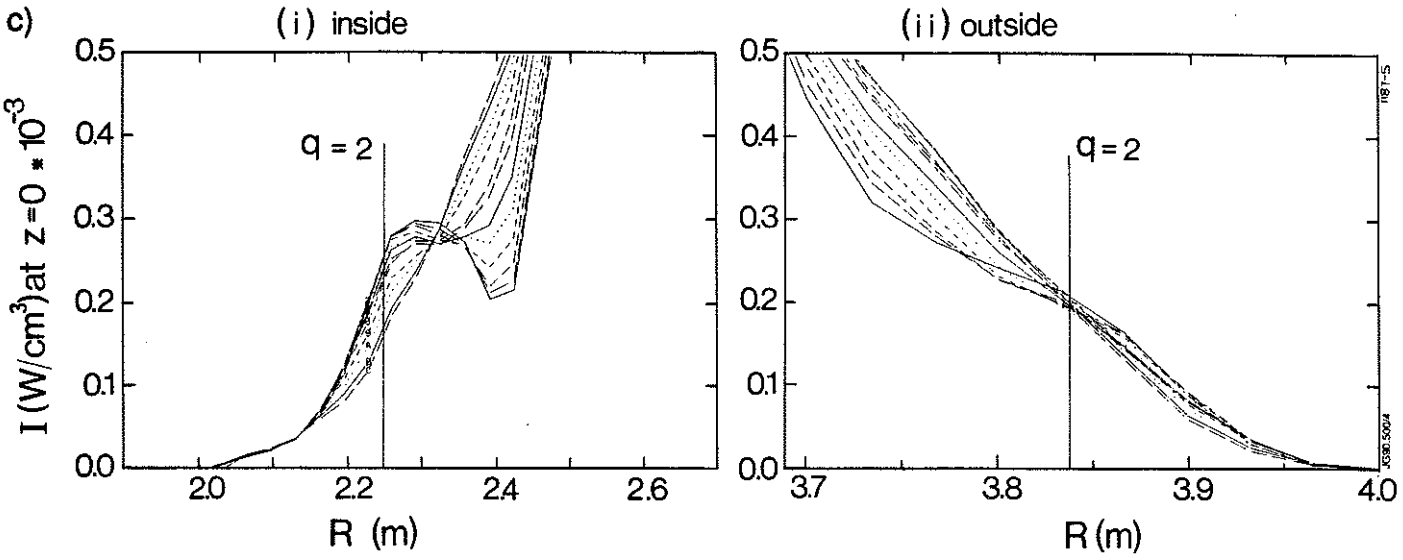

Figure 6 - Observations of a quasi-stationary m=2, n=1 mode

a) - Time traces of magnetic measurements showing:

(i) the amplitude of the radial magnetic field perturbation, b_r, and

(ii) the sine component of b_r.

b) - T_e and q profiles for two times:

(i) t=10 sec,

(ii) t=12 sec.

c) - Radial structure of the soft X-ray midplane emission profile for the q=2 region showing :

(i) high field side, and

(ii) low field side.

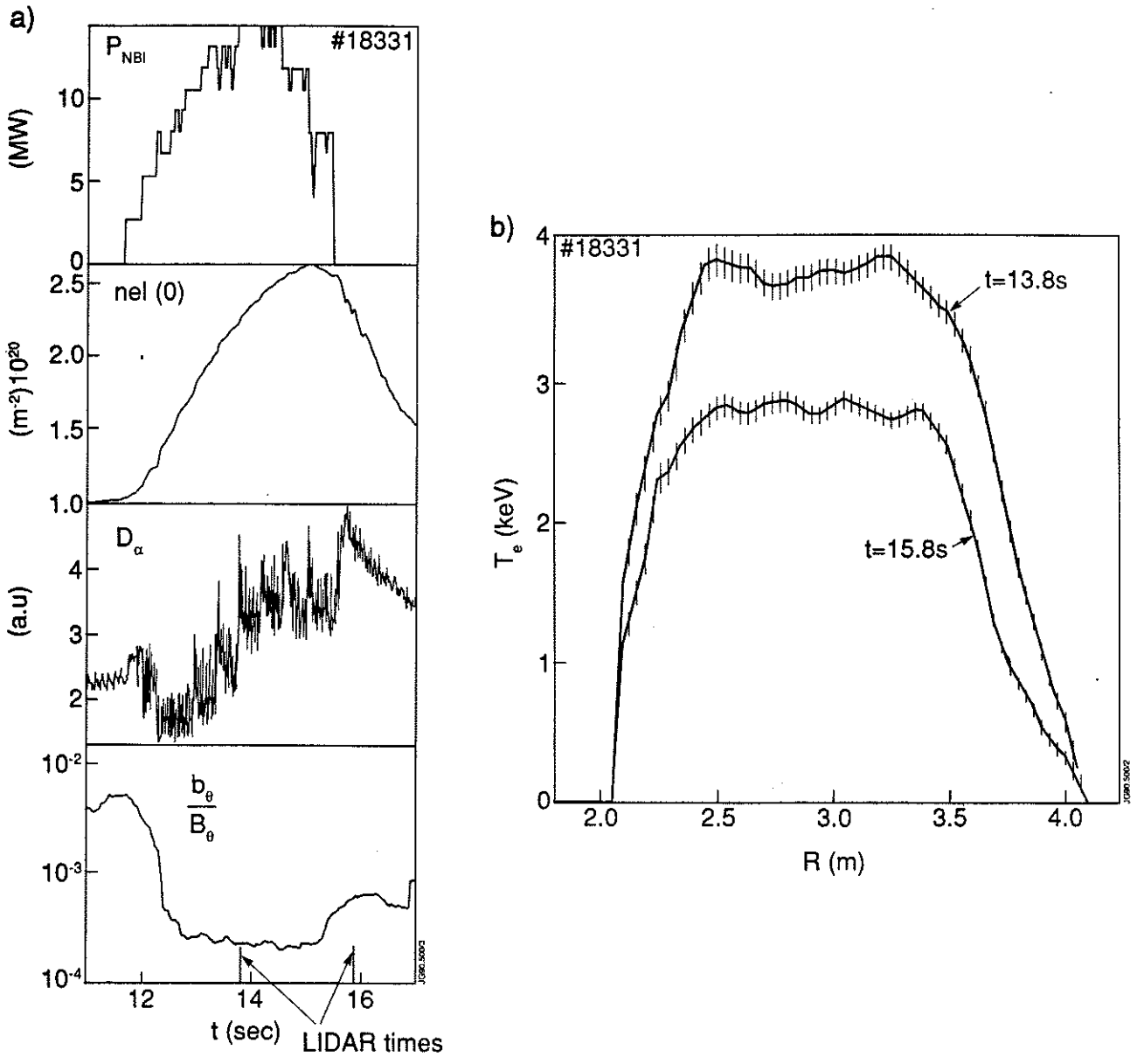

Figure 7- a) Time behavior of plasma parameters during an H-mode:

(i) Total additional power,

(ii) Central line density,

(iii) D_α trace, showing ELMs and sawteeth,

(iv) ratio of perturbed poloidal magnetic field (from a n=1 combination of pick-up coil signals measured at 45° above the mid-plane on the lower field side) to the equilibrium poloidal magnetic field.

b) T_e profiles

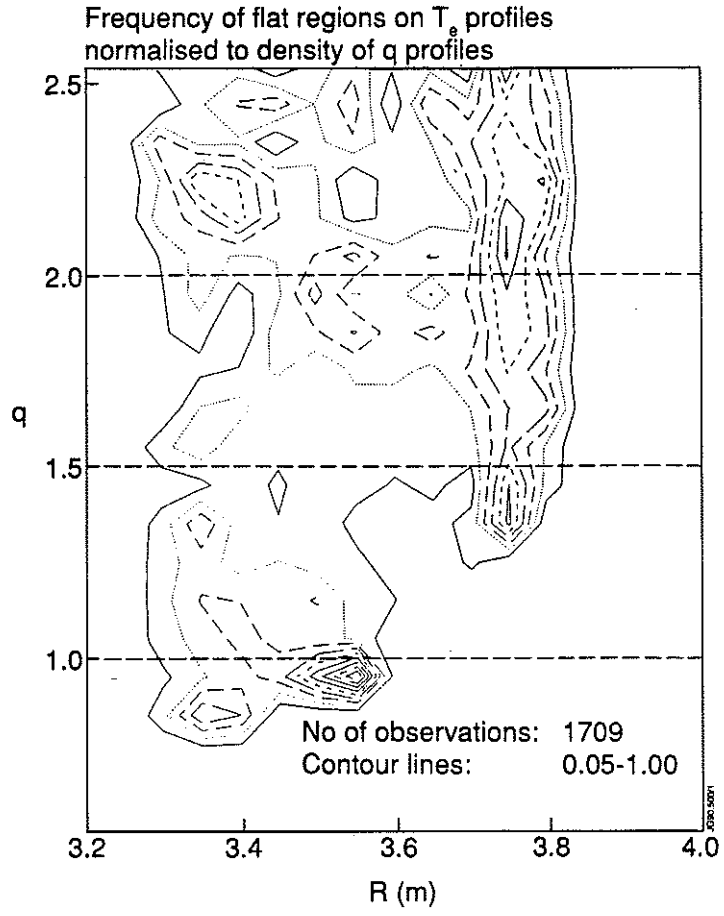

Figure 8 - Contour plots of the frequency of observations in the plane (q,R), for a grid cell size $\Delta q \times \Delta R = 0.1 \times 0.05$cm, normalized to the density of q profiles, for the lower field side. The contour lines start at 0.05 and increase at 0.05 intervals.

APPENDIX 1.

THE JET TEAM

JET Joint Undertaking, Abingdon, Oxon, OX14 3EA, U.K.

J.M.Adams[1], F.Alladio[4], H.Altmann, R.J.Anderson, G.Appruzzese, W.Bailey, B.Balet, D.V.Bartlett, L.R.Baylor[24], K.Behringer, A.C.Bell, P.Bertoldi, E.Bertolini, V.Bhatnagar, R.J.Bickerton, A.Boileau[3], T.Bonicelli, S.J.Booth, G.Bosia, M.Botman, D.Boyd[31], H.Brelen, H.Brinkschulte, M.Brusati, T.Budd, M.Bures, T.Businaro[4], H.Buttgereit, D.Cacaut, C.Caldwell-Nichols, D.J.Campbell, P.Card, J.Carwardine, G.Celentano, P.Chabert[27], C.D.Challis, A.Cheetham, J.Christiansen, C.Christodoulopoulos, P.Chuilon, R.Claesen, S.Clement[30], J.P.Coad, P.Colestock[6], S.Conroy[13], M.Cooke, S.Cooper, J.G.Cordey, W.Core, S.Corti, A.E.Costley, G.Cottrell, M.Cox[7], P.Cripwell[13], F.Crisanti[4], D.Cross, H.de Blank[16], J.de Haas[16], L.de Kock, E.Deksnis, G.B.Denne, G.Deschamps, G.Devillars, K.J.Dietz, J.Dobbing, S.E.Dorling, P.G.Doyle, D.F.Düchs, H.Duquenoy, A.Edwards, J.Ehrenberg[14], T.Elevant[12], W.Engelhardt, S.K.Erents[7], L.G.Eriksonn[5], M.Evrard[2], H.Falter, D.Flory, M.Forrest[7], C.Froger, K.Fullard, M.Gadeberg[11], A.Galetsas, R.Galvao[8], A.Gibson, R.D.Gill, A.Gondhalekar, C.Gordon, G.Gorini, C.Gormezano, N.A.Gottardi, C.Gowers, B.J.Green, F.S.Griph, M.Gryzinski[26], R.Haange, G.Hammett[6], W.Han[9], C.J.Hancock, P.J.Harbour, N.C.Hawkes[7], P.Haynes[7], T.Hellsten, J.L.Hemmerich, R.Hemsworth, R.F.Herzog, K.Hirsch[14], J.Hoekzema, W.A.Houlberg[24], J.How, M.Huart, A.Hubbard, T.P.Hughes[32], M.Hugon, M.Huguet, J.Jacquinot, O.N.Jarvis, T.C.Jernigan[24], E.Joffrin, E.M.Jones, L.P.D.F.Jones, T.T.C.Jones, J.Källne, A.Kaye, B.E.Keen, M.Keilhacker, G.J.Kelly, A.Khare[15], S.Knowlton, A.Konstantellos, M.Kovanen[21], P.Kupschus, P.Lallia, J.R.Last, L.Lauro-Taroni, M.Laux[33], K.Lawson[7], E.Lazzaro, M.Lennholm, X.Litaudon, P.Lomas, M.Lorentz-Gottardi[2], C.Lowry, G.Magyar, D.Maisonnier, M.Malacarne, V.Marchese, P.Massmann, L.McCarthy[28], G.McCracken[7], P.Mendonca, P.Meriguet, P.Micozzi[4], S.F.Mills, P.Millward, S.L.Milora[24], A.Moissonnier, P.L.Mondino, D.Moreau[17], P.Morgan, H.Morsi[14], G.Murphy, M.F.Nave, M.Newman, L.Nickesson, P.Nielsen, P.Noll, W.Obert, D.O'Brien, J.O'Rourke, M.G.Pacco-Düchs, M.Pain, S.Papastergiou, D.Pasini[20], M.Paume[27], N.Peacock[7], D.Pearson[13], F.Pegoraro, M.Pick, S.Pitcher[7], J.Plancoulaine, J-P.Poffé, F.Porcelli, R.Prentice, T.Raimondi, J.Ramette[17], J.M.Rax[27], C.Raymond, P-H.Rebut, J.Removille, F.Rimini, D.Robinson[7], A.Rolfe, R.T.Ross, L.Rossi, G.Rupprecht[14], R.Rushton, P.Rutter, H.C.Sack, G.Sadler, N.Salmon[13], H.Salzmann[14], A.Santagiustina, D.Schissel[25], P.H.Schild, M.Schmid, G.Schmidt[6], R.L.Shaw, A.Sibley, R.Simonini, J.Sips[16], P.Smeulders, J.Snipes, S.Sommers, L.Sonnerup, K.Sonnenberg, M.Stamp, P.Stangeby[19], D.Start, C.A.Steed, D.Stork, P.E.Stott, T.E.Stringer, D.Stubberfield, T.Sugie[18], D.Summers, H.Summers[20], J.Taboda-Duarte[22], J.Tagle[30], H.Tamnen, A.Tanga, A.Taroni, C.Tebaldi[23], A.Tesini, P.R.Thomas, E.Thompson, K.Thomsen[11], P.Trevalion, M.Tschudin, B.Tubbing, K.Uchino[29], E.Usselmann, H.van der Beken, M.von Hellermann, T.Wade, C.Walker, B.A.Wallander, M.Walravens, K.Walter, D.Ward, M.L.Watkins, J.Wesson, D.H.Wheeler, J.Wilks, U.Willen[12], D.Wilson, T.Winkel, C.Woodward, M.Wykes, I.D.Young, L.Zannelli, M.Zarnstorff[6], D.Zasche[14], J.W.Zwart.

PERMANENT ADDRESS

1. UKAEA, Harwell, Oxon. UK.
2. EUR-EB Association, LPP-ERM/KMS, B-1040 Brussels, Belgium.
3. Institute National des Récherches Scientifique, Quebec, Canada.
4. ENEA-CENTRO Di Frascati, I-00044 Frascati, Roma, Italy.
5. Chalmers University of Technology, Göteborg, Sweden.
6. Princeton Plasma Physics Laboratory, New Jersey, USA.
7. UKAEA Culham Laboratory, Abingdon, Oxon. UK.
8. Plasma Physics Laboratory, Space Research Institute, Sao José dos Campos, Brazil.
9. Institute of Mathematics, University of Oxford, UK.
10. CRPP/EPFL, 21 Avenue des Bains, CH-1007 Lausanne, Switzerland.
11. Risø National Laboratory, DK-4000 Roskilde, Denmark.
12. Swedish Energy Research Commission, S-10072 Stockholm, Sweden.
13. Imperial College of Science and Technology, University of London, UK.
14. Max Planck Institut für Plasmaphysik, D-8046 Garching bei München, FRG.
15. Institute for Plasma Research, Gandhinagar Bhat Gujat, India.
16. FOM Instituut voor Plasmafysica, 3430 Be Nieuwegein, The Netherlands.
17. Commissiariat à L'Energie Atomique, F-92260 Fontenay-aux-Roses, France.
18. JAERI, Tokai Research Establishment, Tokai-Mura, Naka-Gun, Japan.
19. Institute for Aerospace Studies, University of Toronto, Downsview, Ontario, Canada.
20. University of Strathclyde, Glasgow, G4 ONG, U.K.
21. Nuclear Engineering Laboratory, Lapeenranta University, Finland.
22. JNICT, Lisboa, Portugal.
23. Department of Mathematics, Univeristy of Bologna, Italy.
24. Oak Ridge National Laboratory, Oak Ridge, Tenn., USA.
25. G.A. Technologies, San Diego, California, USA.
26. Institute for Nuclear Studies, Swierk, Poland.
27. Commissiariat à l'Energie Atomique, Cadarache, France.
28. School of Physical Sciences, Flinders University of South Australia, South Australia SO42.
29. Kyushi University, Kasagu Fukuoka, Japan.
30. Centro de Investigaciones Energeticas Medioambientales y Techalogicas, Spain.
31. University of Maryland, College Park, Maryland, USA.
32. University of Essex, Colchester, UK.
33. Akademie de Wissenschaften, Berlin, DDR.

CR 88.49.1A